

Article

Multiporosity and Multiscale Flow Characteristics of a Stimulated Reservoir Volume (SRV)-Fractured Horizontal Well in a Tight Oil Reservoir

Long Ren ^{1,2,*} , Wendong Wang ^{3,*} , Yuliang Su ³, Mingqiang Chen ^{1,2}, Cheng Jing ^{1,2}, Nan Zhang ^{1,2}, Yanlong He ^{1,2} and Jian Sun ⁴

¹ School of Petroleum Engineering, Xi'an Shiyou University, Xi'an 710065, China; mingqiangchen@163.com (M.C.); cjing@xsyu.edu.cn (C.J.); nanz@xsyu.edu.cn (N.Z.); ylhe@xsyu.edu.cn (Y.H.)

² Shaanxi Key Laboratory of Advanced Stimulation Technology for Oil & Gas Reservoirs, Xi'an 710065, China

³ School of Petroleum Engineering, China University of Petroleum (East China), Qingdao 266580, China; suyuliang@upc.edu.cn

⁴ School of Petroleum Engineering, China University of Petroleum (Beijing), Beijing 102249, China; xjkelsj@163.com

* Correspondence: renlong@xsyu.edu.cn (L.R.); wwdong@upc.edu.cn (W.W.)

Received: 28 August 2018; Accepted: 10 October 2018; Published: 11 October 2018



Abstract: There are multiporosity media in tight oil reservoirs after stimulated reservoir volume (SRV) fracturing. Moreover, multiscale flowing states exist throughout the development process. The fluid flowing characteristic is different from that of conventional reservoirs. In terms of those attributes of tight oil reservoirs, considering the flowing feature of the dual-porosity property and the fracture network system based on the discrete-fracture model (DFM), a mathematical flow model of an SRV-fractured horizontal well with multiporosity and multipermeability media was established. The numerical solution was solved by the finite element method and verified by a comparison with the analytical solution and field data. The differences of flow regimes between triple-porosity, dual-permeability (TPDP) and triple-porosity, triple-permeability (TPTP) models were identified. Moreover, the productivity contribution degree of multimedial was analyzed. The results showed that for the multiporosity flowing states, the well bottomhole pressure drop became slower, the linear flow no longer arose, and the pressure wave arrived quickly at the closed reservoir boundary. The contribution ratio of the matrix system, natural fracture system, and network fracture system during SRV-fractured horizontal well production were 7.85%, 43.67%, and 48.48%, respectively in the first year, 14.60%, 49.23%, and 36.17%, respectively in the fifth year, and 20.49%, 46.79%, and 32.72%, respectively in the 10th year. This study provides a theoretical contribution to a better understanding of multiscale flow mechanisms in unconventional reservoirs.

Keywords: tight oil reservoir; SRV-fractured horizontal well; multiporosity and multiscale; flow regimes; productivity contribution degree of multimedial

1. Introduction

It has been commonly recognized that tight oil reservoirs have threshold pressure gradient and medium deformation characteristics because of their great lithologic compaction, fine pore-throat, and high flow resistance [1–7]. In recent years, stimulated reservoir volume (SRV) fracturing has become the most efficient technology in tight reservoir formation treatment [8–15]. To enhance well production as much as possible, it is necessary to create complex fracture networks with a multiporosity medium by connecting hydraulic fractures with natural fractures away from the well bore, and then increasing

the contact area with formations and reservoir stimulated volume [16–23]. Multiple porous media systems include network fractures, natural fractures, and matrix pore systems. Moreover, there exist different flowing states, i.e., multi-scale flow characteristics.

The research methods of the flow characteristics of SRV-fractured horizontal wells in a tight oil reservoir have been mainly focused on analytical, semi-analytical, and numerical methods. The analytical or semianalytical solution is mainly represented by the three linear flow model proposed by Brown [24], the five-zone model raised by Stalgorova [25], and the compound flow model presented by Su [26]. However, those models have relatively strict assumptions. Generally, the models need to idealize the complex fracture network to regular fracture network forms composed of orthogonal primary and secondary fractures and simplify the complex flow processes to specific flow regimes such as elliptic or linear flow regimes [27–29]. In terms of numerical models, Yao [30] and Fan [31] used the finite element method to carry out dynamic analysis of a horizontal well with a complex fractured continuous medium system, but those models did not consider the development degree of the natural fractures in tight oil reservoirs or the existence of the threshold pressure gradient in the matrix system. Therefore, it is a challenge to use these models to accurately describe the complex structures of actual network fractures and reveal the multiporosity and multiscale flow characteristics of an SRV-fractured horizontal well in tight oil reservoirs.

The objective of this work was to study the multiporosity and multiscale flow characteristics of SRV-fractured horizontal wells. Moreover, the innovation of this paper was to reveal the contribution of multiple porous media to horizontal well productivity by establishing a multiscale flow model. Enlightened by previous studies, a mathematical flow model was built to reflect the multiscale attributes of tight oil reservoirs based on the dual-porosity model (DPM) and discrete-fracture model (DFM), which were divided into three kinds of media systems. A reasonable solution of this numerical model was obtained and verified by the finite element method. Additionally, the flow mechanisms of an SRV-fractured horizontal well with the consideration of the multiporosity and multiscale effect were revealed, which were different to that of a conventional multifractured horizontal well without an SRV system. The findings of this research provide effective theoretical and methodological support for the prediction of the production performance prediction of unconventional hydrocarbon resources.

2. Physical Model and Assumed Conditions

SRV fracturing of a horizontal well in tight oil reservoirs with natural fractures has often induced complex fracture network growth, as revealed by microseismic monitoring [32–35]. Moreover, the complex fracture network divides the reservoir into multiple porous media systems. Furthermore, the physical properties and fluid flow rules of each system are different. Based on the network fracture propagation process and the final form in the tight oil reservoir, a physical model of an SRV fractured horizontal well was built that considered the structure characteristics of multiple porous media, as shown in Figure 1, where Δy_f is the interval between fracturing segments (m); and a and b are the band width and band length of single fracture network, respectively (m).

Complex fracture networks composed of primary and secondary fractures formed by SRV fracturing are integrated into both the natural fracture system and matrix system. A reservoir that has been subjected to SRV fracturing treatment can be represented by a combination of a complex fracture network system, a natural fracture system, and a matrix system. Assumptions of the physical model were made as follows: (1) the study area was a three-dimensional, box-shaped closed, and isotropic body with natural fractures; (2) the rock and fluid were slightly compressible bodies, and the nonlinear flow in the matrix system, Darcy flow in the fracture system, and pseudosteady crossflow between the matrix system and fracture system are also found in the multiple media; and (3) the simulated production process was a single-phase fluid flow in porous and isothermal media without considering the influence of gravity.

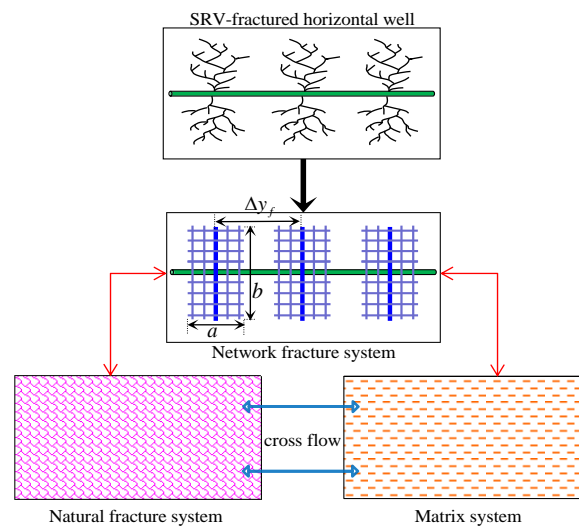


Figure 1. Physical model diagram of the SRV-fractured horizontal well with multi-porosity media.

3. Flow Mathematical Model Considering the Multiporosity

3.1. Nonlinear Flow in the Matrix System

The nonlinear flow equation in the matrix system can be given as [36,37]

$$\mathbf{v}_m = -\frac{\mathbf{K}_m}{\mu} (\nabla p_m - \chi) \quad (1)$$

where \mathbf{v}_m is the flow velocity vector of fluid (10^{-3} m/s); \mathbf{K}_m is the permeability tensor of the matrix (D); μ is the viscosity of fluids (mPa·s); ∇ is the Hamiltonian; p_m is the pore pressure in the matrix system (MPa); χ is the threshold pressure gradient tensor (MPa/m) and can be defined as $\chi = \chi \mathbf{E}$, where χ is the threshold pressure gradient of matrix (MPa/m), and \mathbf{E} is the unit matrix.

Via a combination of the state equation and continuity equation, the surface source in the 3D space is equivalent to the superposition of line sources in the 2D space, and the mathematical flow model for the matrix system can be derived [38] as

$$\nabla^2 p_m - \chi C_L \nabla \cdot p_m - \frac{\phi_m \mu C_m}{K_m} \frac{\partial p_m}{\partial t} - \alpha (p_m - p_n) = 0 \quad (2)$$

where α is the shape factor of matrix; p_n is the pressure of natural fracture (MPa); C_L is the compression coefficient of fluid (MPa^{-1}); and C_m is the comprehensive compression coefficient of matrix system (MPa^{-1}).

Since $C_m = \phi_m C_L + (1 - \phi_m) C_{mf}$ [39], $\phi_m \ll 1$ and $C_{mf} = \phi_m C_p$, the comprehensive compressibility of the matrix system is defined as

$$C_m \approx \phi_m C_L + C_{mf} = \phi_m (C_L + C_p) \quad (3)$$

where ϕ_m is the porosity of the matrix; C_{mf} represents the compression coefficient of the matrix rock (MPa^{-1}); and C_p is the compression coefficient of the pore (MPa^{-1}).

The dimensionless pressure is defined as

$$p_{jD} = \frac{2\pi h_e K_n (p_i - p_j)}{\mu q_j} \quad (4)$$

where j represents m , n , or f ; p_i is the initial formation pressure (MPa); p_j is the pressure of each system (MPa); K_n is the permeability of natural fracture (D); and q_j is the volume flow of each system (s^{-1}).

The dimensionless permeability of the matrix is defined as

$$K_{mD} = K_m / K_n \quad (5)$$

The dimensionless threshold pressure gradient is

$$\chi_D = \chi L C_L \quad (6)$$

The crossflow coefficient between the matrix system and natural fracture system is defined as

$$\lambda = \alpha L^2 K_{mD} \quad (7)$$

The elastic storativity ratio of the natural fracture system is

$$\omega_n = \frac{\phi_n C_n}{\phi_m C_m + \phi_n C_n} \quad (8)$$

where ϕ_n is the porosity of the natural fracture; and C_n is the comprehensive compression coefficient of the natural fracture system (MPa^{-1}).

The dimensionless production time is

$$t_D = \frac{K_n t}{\mu L^2 (\phi_m C_m + \phi_n C_n)} \quad (9)$$

Then, the dimensionless flow equation can be obtained [38] as

$$\nabla^2 p_{mD} - \chi_D \nabla \cdot p_{mD} - (1 - \omega_n) \frac{\partial p_{mD}}{\partial t_D} - \lambda (p_{mD} - p_{nD}) = 0 \quad (10)$$

Accordingly, the initial and boundary condition for fluid flow in the matrix system are given by

$$\begin{cases} p_{mD}(x_D, y_D, z_D; t_D = 0) = 0 \\ \frac{\partial p_{mD}}{\partial x_D} \Big|_{x=x_{eD}} = \frac{\partial p_{mD}}{\partial y_D} \Big|_{y=y_{eD}} = \frac{\partial p_{mD}}{\partial z_D} \Big|_{z_D=z_{eD}} = 0 \end{cases} \quad (11)$$

3.2. Darcy Flow in the Natural Fracture System

Assuming that there exists fluid crossflow between the matrix system and natural fracture system in the formation as well only the natural fracture system instead of the matrix system for fluid exchange to the network fracture system [40], the dimensionless variables are defined as follows: the dimensionless distances are $M_D = M/L$, $M_{eD} = M_e/L$ ($M = x, y, z$), $a_D = a/L$, $b_D = b/L$, where the length, width, and height of the study area are x_e , y_e , and h_e , respectively (m); the horizontal well length is L (m); the dimensionless production rate is $q_{kD} = q_k/q_t$, where k represents n or f ; and q_t is the total volume flow (s^{-1}).

Therefore, the dimensionless Darcy flow equation in the matrix system can be given [31] as

$$\nabla^2 p_{nD} - \omega_n \frac{\partial p_{nD}}{\partial t_D} + \lambda (p_{mD} - p_{nD}) + 2\pi h_{eD} q_{nD} \delta(M - M') = 0 \quad (12)$$

where $\delta(M - M')$ is the Dirac delta function.

The initial and boundary conditions for fluid flow are given by

$$\begin{cases} p_{nD}(x_D, y_D, z_D; t_D = 0) = 0 \\ \frac{\partial p_{nD}}{\partial x_D} \Big|_{x=x_{eD}} = \frac{\partial p_{nD}}{\partial y_D} \Big|_{y=y_{eD}} = \frac{\partial p_{nD}}{\partial z_D} \Big|_{z_D=z_{eD}} = 0 \end{cases} \quad (13)$$

3.3. Darcy Flow in the Network Fracture System

The discrete-fracture model (DFM) is used to characterize the fracture network stimulated system [41,42]. According to the fracture flow model of parallel plate openings (cubic law), the permeability of the network fracture is defined as $K_f = a_f^2/12$, where a_f is the fracture opening (mm). The dimensionless permeability of the network fracture is defined as $K_{fD} = K_f/K_n$; the elastic storativity ratio of the network fracture system is defined as $\omega_f = \phi_f C_f / (\phi_m C_m + \phi_n C_n)$, where ϕ_f is the porosity of the network fracture; and C_f is the comprehensive compression coefficient of the network fracture system (MPa^{-1}).

Similarly, the dimensionless Darcy flow equation in the network fracture system can be given [31] by

$$K_{fD} \nabla^2 p_{fD} - \omega_f \frac{\partial p_{fD}}{\partial t_D} + 2\pi h_{eD} q_{fD} \delta(M - M') = 0 \quad (14)$$

The initial and boundary conditions for fluid flow in the natural fracture system are given by

$$\begin{cases} p_{fD}(x_D, y_D, z_D; t_D = 0) = 0 \\ p_{mD}(x_D, y_D, z_D; t_D) = p_{nD}(x_D, y_D, z_D; t_D) = p_{fD}(x_D, y_D, z_D; t_D) \end{cases} \quad (15)$$

All of the above flow equations and the fixed solution conditions of the matrix, natural fracture, and network fracture systems together constitute the multiporosity and multiscale flow mathematical model for an SRV-fractured horizontal well in tight oil reservoir.

4. Numerical Solution with the Finite Element Method

4.1. Finite Element Method Meshing

The finite element integral equation is established by using Galerkin's weighted residual method and the continuous solving unit with an infinite degree of freedom is discretized into the finite element unit. The horizontal well, network fracture, and reservoir unit are described by a line, triangle, and tetrahedron, respectively. The dimensionless parameters of horizontal wells and hydraulic fractures in a box-shaped closed reservoir are the length of horizontal well $L_D = 1$; the reservoir domain $x_{eD} = 6$, $y_{eD} = 6$, and $h_{eD} = 0.1$; the coordinate of five fracturing sections in the x -direction $(-0.4, 0.2, 0, 0.2, 0.4)$. It is assumed that all fractures are vertical, the mesh generation of the whole model is based on triangle forward algorithm, and local grid refinement (LGR) is performed at the horizontal well and network fracture. The three-dimensional gridding division of an SRV-fractured horizontal well can be obtained as shown in Figure 2.

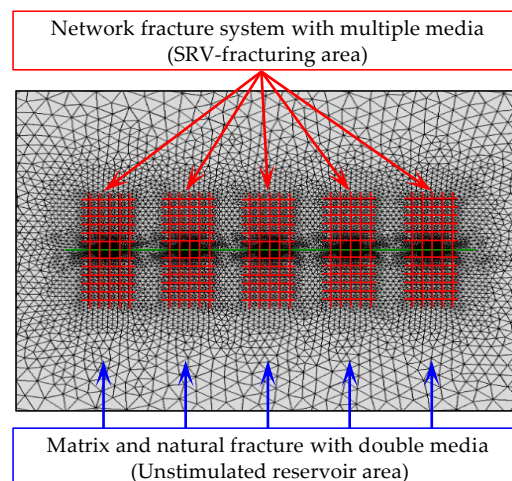


Figure 2. 3D gridding division near an SRV-fractured horizontal well area.

4.2. Finite Element Solution

Assuming that the study area node number is N_p , the node pressure of matrix system and natural fracture system can be written by $\mathbf{P}_m = [P_{m,1}, P_{m,2}, \dots, P_{m,N_p}]^T$ and $\mathbf{P}_n = [P_{n,1}, P_{n,2}, \dots, P_{n,N_p}]^T$. The equivalent integral transformation for control Equations (10), (12), and (14) is carried out by using the equilibrium condition and variation principle, and the characteristic matrix equation of the system element can be obtained. The element characteristic matrix of the network fracture system can be expressed [38] as

$$\begin{aligned} & a_{fD} K_{fD} \iint_{\Omega_{e,f}} \nabla \mathbf{N}_{e,f}^T \nabla \mathbf{N}_{e,f} d\Omega_{e,f} \mathbf{P}_{e,f} + a_{fD} \omega_f \iint_{\Omega_{e,f}} \mathbf{N}_{e,f}^T \mathbf{N}_{e,f} d\Omega_{e,f} \frac{\partial \mathbf{P}_{e,f}}{\partial t_D} \\ & = a_{fD} 2\pi h_D \iint_{\Omega_{e,f}} q_{fD} \mathbf{N}_{e,f}^T \delta(M_D - M'_D) d\Omega_{e,f} \end{aligned} \quad (16)$$

where a_{fD} is the dimensionless opening of the 2D fracture surface; $\mathbf{P}_{e,f}$ is the pressure matrix of the node in the network fracture system; $\Omega_{e,f}$ is the flow area of the network fracture located at the node; and $\mathbf{N}_{e,f} = [N_1, N_2, N_3]$ represents the shape function of two-dimensional triangular elements.

Finally, based on the element characteristic matrix of the matrix system and natural fracture system, the equilibrium equation of the reservoir system can be derived [38] as

$$\mathbf{A}_m \mathbf{P}_m + \mathbf{B}_m \frac{\partial \mathbf{P}_m}{\partial t_D} + \mathbf{C}(\mathbf{P}_m - \mathbf{P}_n) = 0 \quad (17)$$

$$\mathbf{A}_n \mathbf{P}_n + \mathbf{B}_n \frac{\partial \mathbf{P}_n}{\partial t_D} - \mathbf{C}(\mathbf{P}_m - \mathbf{P}_n) = \mathbf{Q}_n \quad (18)$$

where the expression of the coefficient matrix is

$$\begin{aligned} \mathbf{A}_m &= \iiint_{\Omega_{e,mn}} (\nabla \mathbf{N}_{e,mn}^T \nabla \mathbf{N}_{e,mn} + \chi_D \mathbf{N}_{e,mn}^T \nabla \mathbf{N}_{e,mn}) d\Omega_{e,mn} + a_{fD} K_{fD} \iint_{\Omega_{e,f}} \nabla \mathbf{N}_{e,f}^T \nabla \mathbf{N}_{e,f} d\Omega_{e,f} \\ \mathbf{A}_n &= \iiint_{\Omega_{e,mn}} \nabla \mathbf{N}_{e,mn}^T \nabla \mathbf{N}_{e,mn} d\Omega_{e,mn} + a_{fD} K_{fD} \iint_{\Omega_{e,f}} \nabla \mathbf{N}_{e,f}^T \nabla \mathbf{N}_{e,f} d\Omega_{e,f} \\ \mathbf{B}_m &= (1 - \omega_n) \iiint_{\Omega_{e,mn}} \mathbf{N}_{e,mn}^T \mathbf{N}_{e,mn} d\Omega_{e,mn} + a_{fD} \omega_f \iint_{\Omega_{e,f}} \mathbf{N}_{e,f}^T \mathbf{N}_{e,f} d\Omega_{e,f} \\ \mathbf{B}_n &= \omega_n \iiint_{\Omega_{e,mn}} \mathbf{N}_{e,mn}^T \mathbf{N}_{e,mn} d\Omega_{e,mn} + a_{fD} \omega_f \iint_{\Omega_{e,f}} \mathbf{N}_{e,f}^T \mathbf{N}_{e,f} d\Omega_{e,f} \\ \mathbf{C} &= \lambda \iiint_{\Omega_{e,mn}} \mathbf{N}_{e,mn} \mathbf{N}_{e,n}^T d\Omega_{e,mn} \\ \mathbf{Q}_n &= 2\pi h_D \iiint_{\Omega_{e,n}} q_{nD} \mathbf{N}_{e,mn}^T \delta(M_D - M'_D) d\Omega_{e,mn} + a_{fD} 2\pi h_D \iint_{\Omega_{e,f}} q_{fD} \mathbf{N}_{e,f}^T \delta(M_D - M'_D) d\Omega_{e,f} \end{aligned}$$

Assuming that the fluid flows from the natural fracture system to the network fracture system in the initial time, by using the implicit backward difference method concerning time for the equilibrium Equation (18) of the natural fracture system, the governing equation of the finite element method corresponding to the $(k + 1)$ th time of the fracture system can be obtained [38] by

$$\left\{ \mathbf{A}_n + \frac{\mathbf{B}_n}{t_D^{k+1} - t_D^k} + \mathbf{C} \right\} \mathbf{P}_n^{k+1} = \mathbf{Q}_n^{k+1} + \frac{\mathbf{B}_n}{t_D^{k+1} - t_D^k} \mathbf{P}_n^k + \mathbf{C} \mathbf{P}_m^k \quad (19)$$

According to the Equation (17), the pressure of the matrix system at $(k + 1)$ th time step can be calculated as

$$\left\{ \mathbf{A}_m + \frac{\mathbf{B}_m}{t_D^{k+1} - t_D^k} + \mathbf{C} \right\} \mathbf{P}_m^{k+1} = \frac{\mathbf{B}_m}{t_D^{k+1} - t_D^k} \mathbf{P}_m^k + \mathbf{C} \mathbf{P}_n^k \quad (20)$$

When the coefficient matrix $\mathbf{A}_m = 0$, the model represents the triple-porosity, dual-permeability (TPDP) media. When $\mathbf{A}_m \neq 0$, the abovementioned represents the triple-porosity, triple-permeability (TPTP) model. Using the abovementioned dominating Equations (12) and (13), the transient pressure and production performance of an SRV-fractured horizontal well under the conditions of constant productivity rate and stable bottomhole pressure can be calculated respectively.

5. Multiscale Flow Characteristics of SRV-Fractured Horizontal Well

In recent years, SRV fracturing technology has been widely used in the tight oil reservoirs of the Longdong oilfield, Ordos Basin, China. The Chang-7 oil reservoir in the mining area, which has an average depth of 1705 m, is a typical lithologically controlled oil reservoir characterized by tight pores, low pressure, and well-developed natural fractures. Therefore, complex fracture networks with multiple pores are easily developed in the formation after fracturing. According to the actual geological parameters and microseismic monitoring data of a ZP1 horizontal well with SRV fracturing of tight oil reservoirs in the Longdong oilfield, the basic parameters were determined (Table 1). The dimensionless variables used for the analysis and discussion of the results can be calculated, as shown in Table 2. The above parameters were substituted into the dominating Equations (12) and (13) to verify the finite element solution of the proposed model. Furthermore, the flow regimes and production performance of an SRV-fractured horizontal well with multiporosity media were analyzed.

Table 1. Geological and engineering parameters of the ZP1 well in the Longdong oilfield.

Geological and Engineering Parameters, Symbol (Unit)	Value
Reservoir size, $x_e \times y_e \times h_e$ (m)	2400 × 2400 × 40
Permeability, K_m, K_n, K_f (mD)	0.16, 160, 3.33×10^8
Porosity, ϕ_m, ϕ_n, ϕ_f	0.091, 0.27, 0.32
Compression coefficient of fluid and pore, C_L, C_p (MPa ⁻¹)	0.0014, 0.0042
Comprehensive compression coefficient of fracture system, C_n, C_f (MPa ⁻¹)	0.00061, 0.00061
Viscosity of fluids, μ (mPa·s)	1
Threshold pressure gradient, χ (MPa/m)	0.0025
Initial formation pressure, p_i (MPa)	20
Horizontal well length, L (m)	400
Number of fracturing segments, N	5
Segments spacing, Δy_f (m)	80
Network fracture size, $a_D \times b_D$ (m)	40 × 80
Fracture opening, a_f (mm)	2

Table 2. Dimensionless variables used for the analysis and discussion of the results.

Dimensionless Parameters, Symbol	Value
Reservoir size, $x_{eD} \times y_{eD} \times h_{eD}$	6 × 6 × 0.1
Network fracture size, $a_D \times b_D$	0.1 × 0.2
Fracture opening, a_{fD}	0.5×10^{-6}
Matrix permeability, K_{mD}	0.001
Network fracture permeability, K_{fD}	2.08×10^6
Threshold pressure gradient, χ_D	0.001
Elastic storativity ratio of the natural fracture system, ω_n	0.78
Elastic storativity ratio of network fracture system, ω_f	0.92
Crossflow coefficient, λ	60

5.1. Accuracy Verification of the Numerical Solution

To verify the accuracy of the numerical solution of our model, on the one hand, it was considered that the reservoir was a dual-porosity and single-permeability medium without threshold pressure. Moreover, only primary fractures exist in the reservoir after fracturing. The numerical solution of the finite element model was compared with the analytical solution of the Zerzar et al. 2004 model [43] for a conventional multistage fractured horizontal well, and the comparative curve of the pressure and pressure derivative behaviors were obtained, as shown in Figure 3. On the other hand, according to the actual geological parameters and fracturing parameters of a ZP1 well with 33 months of production history in the Longdong oilfield, the oil production rate and cumulative oil production of the ZP1 well with SRV fracturing could be calculated using the numerical model proposed in this paper, and the comparison curves are shown in Figure 4.

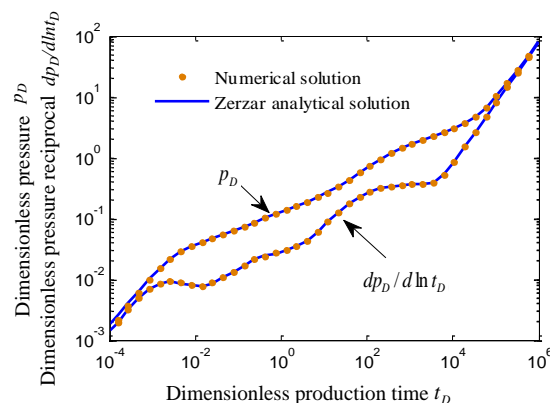


Figure 3. Pressure and pressure derivative behaviors in a multi-stage fractured horizontal well intercepted by the numerical solution and Zerzar [43] analytical solution.

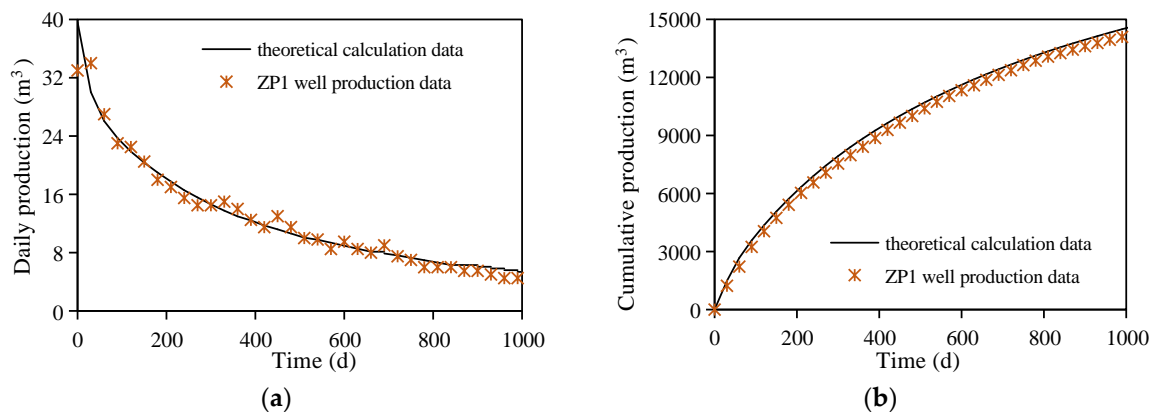


Figure 4. Comparison curve of the ZP1 well production data and theoretical calculation data. (a) Oil production rate. (b) Cumulative oil production.

Figure 3 shows that the pressure and pressure derivative behaviors of a multistage fractured horizontal well calculated by the two models were basically consistent. Figure 4 shows that the theoretical model had good degree of fit with the actual well production data. Therefore, the model established in this paper could not only be simplified as the Zerzar analytical solution model, but could also be used to accurately predict the production performance of an SRV-fractured well in tight oil reservoirs.

5.2. Flow Regimes Division during Well Production

Considering the effect of natural fractures inherent in tight formation and network fracture systems produced by SRV fracturing on the productivity of the horizontal well and using the TPDP and TPTP models to simulate the production performance of a horizontal well under the conditions of constant productivity rate, the pressure, and pressure derivative behaviors (type-curves of well testing) [44] for an SRV-fractured horizontal well in a tight oil reservoir could be obtained, as shown in Figure 5.

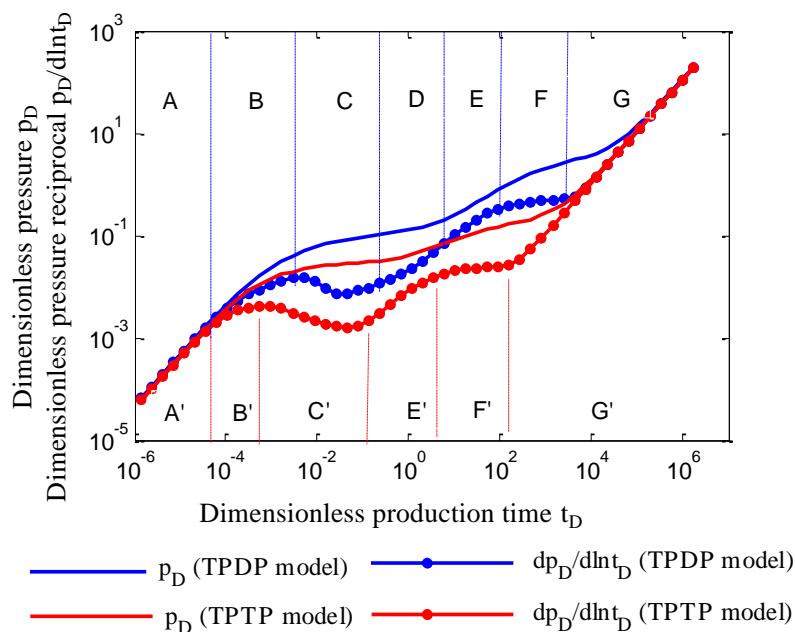


Figure 5. Type-curves of well testing for an SRV-fractured horizontal well with the TPDP and TPTP models.

For the TPDP model, the matrix system exhibited only the fluid crossflow phenomenon with the natural fracture system, but was not involved in the fluid flow process to the network fracture system. Under the assumption that the stimulated area was composed of triple-porosity media and the unstimulated area was composed of dual-porosity media, based on the pressure derivative curve, the TPDP model flow regimes during SRV-fractured horizontal well production in a tight oil reservoir could be divided into seven flow periods, as shown in Figure 6, where k is the slope of the pressure derivative curve; and both m and n are constants.

The TPDP model flow regimes can be divided into the following periods. Stage A: The initial pseudosteady flow around primary fractures; this stage mainly reflects the linear flow inside the primary fractures and the radial flow around the primary fractures, and the combination of the two causes the pressure derivative behavior to show a straight line with unit slope. Stage B: Linear flow inside the network fracture system; this stage reflects the linear flow from the secondary fractures to the primary fracture, and the pressure derivative behavior shows an oblique line with a near unit slope. Stage C: Pseudosteady crossflow between the matrix and natural fracture systems; as the pressure drop of the natural fracture system is greater than that of the matrix system, this stage mainly reflects the pseudosteady flow process from the matrix system into the natural fracture system, which leads to a concave part of the pressure derivative behavior. Stage D: Formation linear flow; this stage represents the linear flow around the network fracture, and the pressure derivative curve shows a straight line with a $1/2$ slope. Stage E: Pseudosteady flow in the stimulated area; when the pressure wave propagates to the boundary of the stimulated area, the effective distance of fluid flow in the unstimulated area increases continuously, resulting in the formation of a moving sealed boundary

with time changing around the stimulated areas. The pressure derivative behavior shows an oblique line with a near unit slope. Stage F: Pseudo radial flow near the SRV-fractured horizontal well; the flow characteristics at this stage are expressed as a pseudo radial flow centered on the horizontal well with the network fracture system, and the pressure derivative behavior is shown as a horizontal straight line. Stage G: Pseudosteady flow in the whole reservoir; the influence of the closed outer boundary is observed during the later stage of well production, i.e., when the pressure wave propagates to the reservoir boundary, the bottomhole pressure drops rapidly and pressure derivative behavior is shown as a straight line with unit slope.

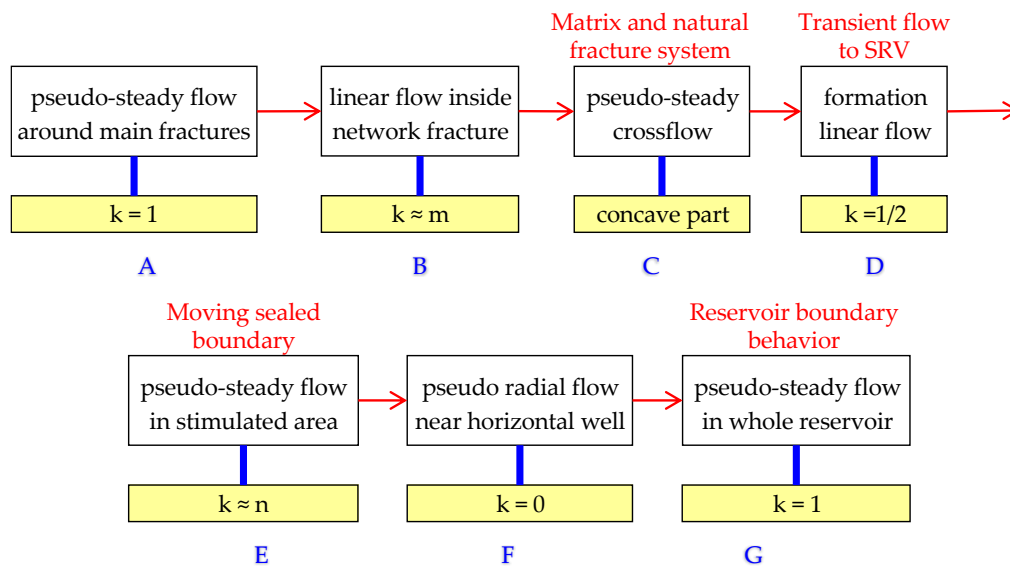


Figure 6. Flow regimes division during SRV-fractured horizontal well production in tight oil reservoir.

For the TPTP model, the fluid in the matrix system is involved in the flow to the network fracture system. Therefore, comparing with the TPDP model flow regimes, the bottomhole pressure drop of the horizontal well with the TPTP model becomes slower in the B', C', E', and F' stages. The linear flow in the formation (D) no longer arises and is covered by the pseudosteady crossflow (C'), which quickly changes the pseudosteady flow (E'). Then, the pressure wave propagates quickly to the closed reservoir boundary, and the bottomhole pressure drop increases rapidly during the pseudosteady flow in the whole reservoir (G'), which is consistent with the pressure and pressure derivative behaviors of the TPDP model gradually. According to the development experience of tight oil reservoirs, the TPTP model is more reasonable for tight oil reservoir simulation.

5.3. Productivity Contribution Degree of Multiporosity Systems

To further quantitatively analyze the contribution degree of multiporosity systems to well productivity, the TPTP model was used to simulate the production process of the SRV-fractured horizontal well (800 m in length and fracturing with 10 segments) under the following three cases: (1) there was only the matrix system in the reservoir; (2) there were only the matrix and natural fracture systems in reservoirs; (3) there were the matrix, natural fracture, and network fracture systems in the reservoirs. The productivity (including the daily production and cumulative production) contribution curves for the three systems (including the matrix, natural fracture, and network fracture systems) during SRV-fractured horizontal well production in tight oil reservoirs can be calculated respectively, as shown in Figure 7. Moreover, the daily production contribution ratio (DPCR) and cumulative production contribution ratio (CPCR) of the three systems to SRV-fractured horizontal well productivity can be obtained statistically, as shown in Table 3.

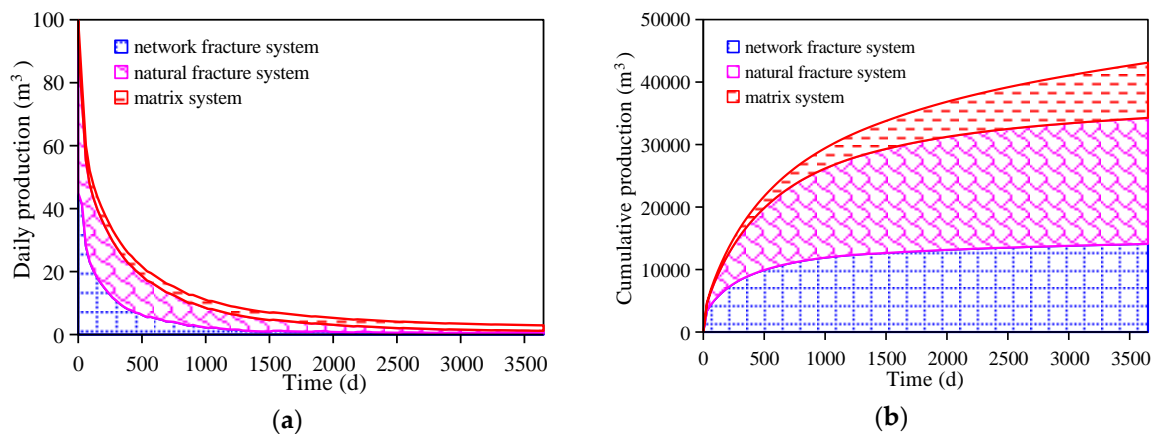


Figure 7. Productivity contribution curves of three systems during SRV-fractured horizontal well production in a tight oil reservoir. (a) Oil production rate. (b) Cumulative oil production.

Table 3. DPCR and CPCR of three systems to SRV-fractured horizontal well productivity in different development stages of tight oil reservoir

DPCR ¹ (%)	Matrix System	Natural Fracture System	Network Fracture System
CPCR ² (%)			
1st year	11.73	56.36	31.91
	7.85	43.67	48.48
5th year	39.08	45.49	15.43
	14.60	49.23	36.17
10th year	59.12	26.80	14.08
	20.49	46.79	32.72

¹ DPCR is the daily production contribution ratio; ² CPCR is the cumulative production contribution ratio.

The simulation results indicated that the proportion of productivity contribution for triple-porosity media systems during SRV-fractured horizontal well production varied at different stages of reservoir development. In the early stage of tight oil reservoir development, the productivity of the SRV-fractured horizontal well was mainly contributed to by natural fracture and network fracture systems with high conductivity. The daily production rate was large, but declined rapidly. After that stage, due to the fracture failure, the DPCR of the natural fracture and network fracture systems gradually decreased, and the latter was more serious; on the contrary, the DPCR of matrix system increased rapidly. In the late stage of reservoir development, the daily production of the horizontal well was maintained at a lower level, and the DPCR of the matrix system was more than half. The CPCR of the matrix system, natural fracture system, and network fracture system during SRV-fractured horizontal well production were 7.85%, 43.67%, and 48.48%, respectively in the 1st year; 14.60%, 49.23%, and 36.17%, respectively in the 5th year; and 20.49%, 46.79%, and 32.72%, respectively in the 10th year.

6. Conclusions

During the development of a tight oil reservoir after SRV fracturing, the flow characteristics are different from those of conventional reservoirs. This paper investigated the multiporosity and multiscale flow characteristics of an SRV-fractured horizontal well in a tight oil reservoir. Based on the dual-media theory and discrete-fracture network models, a mathematical flow model of an SRV-fractured horizontal well with multiporosity and multipermeability media was built, solved, and verified. It has been found that there exist different flow regimes and productivity characteristics in SRV-fractured horizontal wells. The TPDP model flow regimes during SRV-fractured horizontal well production in tight oil reservoirs could be divided into seven flow periods, which include the initial pseudosteady flow around the primary fractures, linear flow inside the network fracture

system, pseudosteady crossflow, formation linear flow, pseudosteady flow in the stimulated area, pseudoradial flow near horizontal well, and pseudosteady flow in the whole reservoir. For the multiporosity and multiscale flowing states, the well bottomhole pressure drop became slower, the linear flow in the formation no longer arose, and the pressure wave arrived quickly at the closed reservoir boundary. The initial production rate of the SRV-fractured horizontal well was large but declined rapidly. The contribution ratio of the matrix system, natural fracture system, and network fracture system during SRV-fractured horizontal well production were 7.85%, 43.67%, and 48.48%, respectively in the 1st year; 14.60%, 49.23%, and 36.17%, respectively in the 5th year; and 20.49%, 46.79%, and 32.72%, respectively in the 10th year. The proposed research may provide valuable insight into understanding the multiporosity and multiscale flow mechanisms and unconventional hydrocarbon recovery maximization. For the actual oilfield, the change of the dynamic energy of the formation system can be predicted by the change of well productivity, which could guide managers in carrying out the development of regime adjustment and improvements in the management system in a timely manner.

Author Contributions: L.R. and W.W. conceived the strategy and designed the theoretical framework; Y.S., M.C., C.J. and N.Z. conducted the simulations and analyzed the data; L.R., Y.H., and J.S. wrote the manuscript; and all authors have read and approved the final manuscript.

Funding: This research was supported by the National Natural Science Foundation of China (no. 51704235, 51804328, 51874242), Young Talent fund of University Association for Science and Technology in Shaanxi, China (no. 20180417), Shandong Province Natural Science Foundation (ZR2018BEE008), Fundamental Research Funds for the Central Universities (18CX02168A) and Natural Science Basic Research Plan in Shaanxi Province of China (no. 2018JQ5208).

Acknowledgments: The authors appreciate the reviewers and editors for their critical and helpful comments.

Conflicts of Interest: The authors declare no conflict of interest.

References

1. Jia, C.Z.; Zheng, M.; Zhang, Y.F. Unconventional hydrocarbon resources in China and the prospect of exploration and development. *Pet. Explor. Dev.* **2012**, *39*, 129–136. [[CrossRef](#)]
2. Wang, W.D.; Zheng, D.; Sheng, G.L.; Zhang, Q.; Su, Y.L. A review of stimulated reservoir volume characterization for multiple fractured horizontal well in unconventional reservoirs. *Adv. Geo-Energy Res.* **2017**, *1*, 54–63. [[CrossRef](#)]
3. Singh, H.; Cai, J.C. A mechanistic model for multi-scale sorption dynamics in shale. *Fuel* **2018**, *234*, 996–1014. [[CrossRef](#)]
4. Ren, L.; Su, Y.L.; Zhao, G.Y. Non-Darcy flow pattern response and critical well spacing in tight oil reservoirs. *J. Cent. South Univ.* **2015**, *5*, 1732–1738. [[CrossRef](#)]
5. Wu, Q.; Xu, Y.; Zhang, S.L.; Wang, T.F.; Guan, B.S.; Wu, G.T.; Wang, X.Q. The core theories and key optimization designs of volume stimulation technology for unconventional reservoirs. *Acta Pet. Sin.* **2014**, *35*, 706–714. [[CrossRef](#)]
6. Liu, G.; Meng, Z.; Cui, Y.; Wang, L.; Liang, C.; Yang, S. A Semi-Analytical Methodology for Multiwell Productivity Index of Well-Industry-Production-Scheme in Tight Oil Reservoirs. *Energies* **2018**, *11*, 1054. [[CrossRef](#)]
7. Wang, W.D.; Su, Y.L.; Yuan, B.; Wang, K.; Cao, X.P. Numerical simulation of fluid flow through fractal-based discrete fractured network. *Energies* **2018**, *11*, 286. [[CrossRef](#)]
8. Tang, C.; Chen, X.; Du, Z.; Yue, P.; Wei, J. Numerical Simulation Study on Seepage Theory of a Multi-Section Fractured Horizontal Well in Shale Gas Reservoirs Based on Multi-Scale Flow Mechanisms. *Energies* **2018**, *11*, 2329. [[CrossRef](#)]
9. Zhang, Q.; Su, Y.; Wang, W.; Lu, M.; Ren, L. Performance analysis of fractured wells with elliptical SRV in shale reservoirs. *J. Nat. Gas Sci. Eng.* **2017**, *45*, 380–390. [[CrossRef](#)]
10. Yao, J.; Sun, H.; Li, A.F.; Yang, Y.F.; Huang, Z.Q.; Wang, Y.Y.; Zhang, L.; Kou, J.L.; Xie, H.J.; Zhao, J.L.; et al. Modern system of multiphase flow in porous media and its development trend. *Chin. Sci. Bull.* **2018**, *63*, 425–451. [[CrossRef](#)]

11. Mayerhofer, M.J.; Lonon, E.; Warpinski, N.R.; Cipolla, C.L.; Walser, D.W.; Rightmire, C.M. What is stimulated reservoir volume? *SPE Prod. Oper.* **2010**, *25*, 89–98. [[CrossRef](#)]
12. Chong, Z.; Li, X.; Chen, X.; Zhang, J.; Lu, J. Numerical investigation into the effect of natural fracture density on hydraulic fracture network propagation. *Energies* **2017**, *10*, 914. [[CrossRef](#)]
13. Wang, W.D.; Su, Y.L.; Zhang, X.; Sheng, G.L. Analysis of the complex fracture flow in multiple fractured horizontal wells with the fractal tree-like network models. *Fractals Complex Geom. Patterns Scaling Nat. Soc.* **2015**, *23*, 1550014. [[CrossRef](#)]
14. Wu, Q.; Xu, Y.; Wang, X.Q.; Wang, T.F.; Zhang, S.L. Volume fracturing technology of unconventional reservoirs: Connotation, optimization design and implementation. *Pet. Explor. Dev.* **2012**, *39*, 352–358. [[CrossRef](#)]
15. Yuan, B.; Zheng, D.; Moghanloo, R.G.; Wang, K. A novel integrated workflow for evaluation, optimization, and production prediction in shale plays. *Int. J. Coal Geol.* **2017**, *180*, 18–28. [[CrossRef](#)]
16. Wang, Y.; Li, X.; He, J.; Zhao, Z.; Zheng, B. Investigation of fracturing network propagation in random naturally fractured and laminated block experiments. *Energies* **2016**, *9*, 588. [[CrossRef](#)]
17. Kaustubh, S.; Sharma, M.M. Mechanisms for the formation of complex fracture networks in naturally fractured rocks. In Proceedings of the SPE Hydraulic Fracturing Technology Conference and Exhibition, The Woodlands, TX, USA, 23–25 January 2018. [[CrossRef](#)]
18. Cai, J.C.; Wei, W.; Hu, X.Y.; Liu, R.C.; Wang, J.J. Fractal characterization of dynamic fracture network extension in porous media. *Fractals* **2017**, *25*, 1750023. [[CrossRef](#)]
19. Su, Y.; Sheng, G.; Wang, W.; Zhang, Q.; Lu, M.; Ren, L. A mixed-fractal flow model for stimulated fractured vertical wells in tight oil reservoirs. *Fractals* **2016**, *24*, 1650006. [[CrossRef](#)]
20. Zeng, F.; Cheng, X.; Guo, J.; Chen, Z.; Xiang, J. Investigation of the initiation pressure and fracture geometry of fractured deviated wells. *J. Pet. Sci. Eng.* **2018**, *165*, 412–427. [[CrossRef](#)]
21. Ren, L.; Su, Y.; Zhan, S.; Hao, Y.; Meng, F.; Sheng, G. Modeling and simulation of complex fracture network propagation with SRV fracturing in unconventional shale reservoirs. *J. Nat. Gas Sci. Eng.* **2016**, *28*, 132–141. [[CrossRef](#)]
22. Zhang, Q.; Su, Y.; Wang, W.; Sheng, G. A new semi-analytical model for simulating the effectively stimulated volume of fractured wells in tight reservoirs. *J. Nat. Gas Sci. Eng.* **2015**, *27*, 1834–1845. [[CrossRef](#)]
23. Weng, D.W.; Lei, Q.; Xu, Y.; Li, Y.; Li, D.Q.; Wang, W.X. Network fracturing techniques and its application in the field. *Acta Pet. Sin.* **2011**, *32*, 281–284. [[CrossRef](#)]
24. Brown, M.; Ozkan, E.; Raghavan, R.; Kazemi, H. Practical solutions for pressure transient responses of fractured horizontal wells in unconventional reservoirs. In Proceedings of the SPE Annual Technical Conference and Exhibition, New Orleans, LA, USA, 4–7 October 2009. [[CrossRef](#)]
25. Stalgorova, E.; Mattar, L. Analytical model for unconventional multifractured composite systems. *SPE Reserv. Eval. Eng.* **2013**, *3*, 246–256. [[CrossRef](#)]
26. Su, Y.L.; Wang, W.D.; Sheng, G.L. Compound flow model of volume fractured horizontal well. *Acta Pet. Sin.* **2014**, *35*, 504–510. [[CrossRef](#)]
27. Xu, W.Y.; Li, J.; Du, M. Quick estimate of initial production from stimulated reservoirs with complex hydraulic fracture network. In Proceedings of the SPE Annual Technical Conference and Exhibition, Denver, CO, USA, 30 October–2 November 2011. [[CrossRef](#)]
28. Jia, P.; Cheng, L.S.; Huang, S.J.; Xue, Y.C.; Ai, S. Production simulation of complex fracture networks for shale gas reservoirs using a semi-analytical model. In Proceedings of the SPE Asia Pacific Unconventional Resources Conference and Exhibition, Brisbane, Australia, 9–11 November 2015. [[CrossRef](#)]
29. Yang, R.Y.; Huang, Z.W.; Yu, W.; Lashgari, H.R.; Sepehrnoori, K.; Shen, Z.H. A semianalytical method for modeling two-phase flow in coalbed methane reservoirs with complex fracture networks. In Proceedings of the SPE/AAPG/SEG Unconventional Resources Technology Conference, San Antonio, TX, USA, 1–3 August 2016. [[CrossRef](#)]
30. Yao, J.; Yin, X.X.; Fan, D.Y.; Sun, Z.X. Trilinear flow well test model of fractured horizontal well in low permeability reservoir. *Well Test.* **2011**, *20*, 1–5. [[CrossRef](#)]
31. Fan, D.Y.; Yao, J.; Sun, H.; Zeng, H.; Wang, W. A composite model of hydraulic fractured horizontal well with stimulated reservoir volume in tight oil & gas reservoir. *J. Nat. Gas Sci. Eng.* **2015**, *24*, 115–123. [[CrossRef](#)]

32. Fisher, M.K.; Wright, C.A.; Davidson, B.M.; Steinsberger, N.P.; Buckler, W.S.; Goodwin, A.; Fielder, E.O. Integrating fracture mapping technologies to improve stimulations in the Barnett shale. *SPE Prod. Facil.* **2005**, *20*, 85–93. [[CrossRef](#)]
33. Daniels, J.L.; Waters, G.A.; Le Calvez, J.H.; Bentley, D.; Lassek, J.T. Contacting more of the Barnett shale through an integration of real-time microseismic monitoring petrophysics and hydraulic fracture design. In Proceedings of the SPE Annual Technical Conference and Exhibition, Anaheim, CA, USA, 11–14 November 2007. [[CrossRef](#)]
34. Maxwell, S.C.; Urbancic, T.I.; Steinsberger, N.; Zinno, R. Microseismic imaging of hydraulic fracture complexity in the Barnett shale. In Proceedings of the SPE Annual Technical Conference and Exhibition, San Antonio, TX, USA, 29 September–2 October 2002. [[CrossRef](#)]
35. Le Calvez, J.H.; Craven, M.E.; Klem, R.C.; Baihly, J.D.; Bennett, L.A.; Brook, K. Real-time microseismic monitoring of hydraulic fracture treatment: A tool to improve completion and reservoir management. In Proceedings of the SPE Hydraulic Fracturing Technology Conference, College Station, TX, USA, 29–31 January 2007. [[CrossRef](#)]
36. Prada, A.; Civan, F. Modification of Darcy’s law for the threshold pressure gradient. *J. Petrol. Sci. Eng.* **1999**, *22*, 237–240. [[CrossRef](#)]
37. Cai, J.C. A fractal approach to low velocity non-Darcy flow in a low permeability porous medium. *Chin. Phys. B* **2014**, *23*, 044701. [[CrossRef](#)]
38. Ren, L.; Su, Y.L.; Hao, Y.M.; Zhang, Q.; Meng, F.K.; Sheng, G.L. Dynamic analysis of SRV-fractured horizontal wells in tight oil reservoirs based on stimulated patterns. *Acta Pet. Sin.* **2015**, *36*, 1272–1279. [[CrossRef](#)]
39. Hall, H.N. Compressibility of reservoir rocks. *J. Pet. Technol.* **1953**, *5*, 17–19. [[CrossRef](#)]
40. Sun, Z.X.; Yao, J.; Fan, D.Y.; Wang, Y.Y.; Zhang, K.S. Dynamic analysis of horizontal wells with complex fractures based on a discrete-fracture model. *J. China Univ. Pet.* **2014**, *38*, 109–115. [[CrossRef](#)]
41. Yan, B.; Mi, L.; Chai, Z.; Wang, Y.; Killough, J.E. An enhanced discrete fracture network model for multiphase flow in fractured reservoirs. *J. Pet. Sci. Eng.* **2018**, *161*, 667–682. [[CrossRef](#)]
42. Shakiba, M.; Sepehrnoori, K. Using embedded discrete fracture model (EDFM) in numerical simulation of complex hydraulic fracture networks calibrated by microseismic monitoring data. *J. Nat. Gas Sci. Eng.* **2018**, *55*, 495–507. [[CrossRef](#)]
43. Zerzar, A.; Tiab, D.; Bettam, Y. Interpretation of multiple hydraulically fractured horizontal wells. In Proceedings of the Society of Petroleum Engineers Abu Dhabi International Conference and Exhibition, Abu Dhabi, UAE, 10–13 October 2004. [[CrossRef](#)]
44. Zhao, Y.L.; Shan, B.C.; Zhang, L.H.; Liu, Q.G. Seepage flow behaviors of multi-stage fractured horizontal wells in arbitrary shaped shale gas reservoirs. *J. Geophys. Eng.* **2016**, *13*, 674–689. [[CrossRef](#)]



© 2018 by the authors. Licensee MDPI, Basel, Switzerland. This article is an open access article distributed under the terms and conditions of the Creative Commons Attribution (CC BY) license (<http://creativecommons.org/licenses/by/4.0/>).